 doi:10.20944/preprints201812.0136.v1

Article

Analysis of Spatiotemporal Variation of Land Subsidence in Beijing Plain, China

Lin Guo[1,2,3,] *, Huili Gong[1,2,3]*, Feng Zhu[5], Lin Zhu[1,2,3], Chaofan Zhou[1,2,3,4], and Yike Sun[1,2,3]

[1] College of Resources Environment and Tourism, Capital Normal University, 105 North Road of the Western 3rd Ringroad, Haidian District, Beijing 100048, China; 6382@cnu.edu.cn(L.G.); gonghl_1956@163.com (H.G.); hi-zhulin@163.com (L.Z.); B328@cnu.edu.cn(C.Z.); sun_un_yikesyk@163.com(Y.S.)

[2] Key Laboratory of 3D Information Acquisition and Application, MOE, Capital Normal University, Beijing 100048, China

[3] Base of the State Key Laboratory of Urban Environmental Process and Digital Modeling, Capital Normal University, Beijing 100048, China

[4] Beijing Advanced Innovation Center for Imaging Technology, Capital Normal University, Beijing 100048, China

[5] Department of Geography, Yuying School, 11 West Street of Wanshou Road, Haidian District, Beijing 100036, China; zhufeng19851007@163.com

* Correspondence: gonghl_1956@163.com (H.G.); 6382@cnu.edu.cn (L.G.); Tel.: +86-138-1113-8025

Abstract: Since the 1970s, land subsidence has been developing rapidly in the Beijing Plain, the systematic study of its evolution mechanism is of great significance to the sustainable development of the regional economy. First, based on ENVISAT ASAT and RADARSAT2 data, the land subsidence data in Beijing Plain were obtained using permanent interferometer technology. Second, based on the GIS platform and using fishing net tools, vector data of ground settlement with different resolutions were obtained. Through a series of tests, a scale of 960 metres was selected as the research unit, and the subsidence rate of the grid was obtained from 2004 to 2015. Finally, based on the Mann-Kendall mutation test method, a trend analysis of land subsidence changes in various grids was carried out. The results showed that single-year mutation mainly distributed in the middle and lower parts of the Yongding River alluvial fan and the Chaobai River alluvial fan, mainly occurring in 2015, 2005 and 2013, respectively. The upper and middle alluvial fan of the Chaobai River, the vicinity of the emergency water source and the edge velocity of the groundwater funnel have undergone several sudden changes. Combined with hydrogeology, basic geological conditions and the impact of the South-to-North Water transfer project, we analysed the causes of the mutations in the grid. The research results can provide a basis for the study and prevention of land subsidence in this area and help to further explore the trend characteristics of land subsidence in this area.

Keywords: Land subsidence; InSAR; Small baseline interferometry; Mann-Kendall mutation test; Fishnet

1. Introduction

Land subsidence is a geological phenomenon caused by human engineering activities (e.g., groundwater exploitation) or natural factors, and in this phenomenon, the ground elevation is reduced within a certain area [1, 2]. The occurrence of land subsidence is almost irreversible. When severe local surface subsidence occurs, it will induce a series of geological environmental disasters, such as foundation sinking, house cracking and underground pipeline damage [3-5]; furthermore, subsidence has the characteristics of a long formation time, wide influence range and great difficulty in prevention and control. At present, more than 150 countries and regions have suffered land subsidence, which has caused large security risks and economic losses. In China, land subsidence mainly occurs in the North China Plain, the Yangtze River Delta, the Fenwei Basin and the Pearl River

 doi:10.20944/preprints201812.0136.v1

Delta, and the process presents significant regional differences [6-11]. Among them, the continuous land subsidence in the North China Plain (Beijing-Tianjin-Hebei region) continues to increase, the Yangtze River Delta region has been effectively controlled, and the Fenwei Basin region is still developing rapidly.

From the perspective of land subsidence monitoring technology, InSAR technology has become a new ground observation technology in the past 20 years [12-14]. Compared with traditional technology, InSAR technology has the advantages of a wide monitoring range and a high monitoring accuracy, and the technology has been widely used in land subsidence monitoring research by experts and scholars [14-20]. In 2002 and 2004, Berardino and Lanaride et al. proposed the small baseline set interferometry (SBAS-InSAR) technique, which is more suitable for the long-term slow deformation of surface monitoring. Subsequently, experts and scholars used this technology to select multi-source SAR data, such as ENVISAT ASAR and COSMO-SkyMed, and monitored the surface deformation information of Los Angeles, northern California, central Mexico and other areas [1, 21-29]. From the perspective of the evolution mechanism of land subsidence, the causes of the occurrence and evolution of land subsidence include natural factors and human factors [30]. For a long time, experts and scholars have been focusing more on the land subsidence caused by human factors. At present, 80% of land subsidence is caused by the excessive exploitation of groundwater fluid resources [31].

Beijing, as the capital of China, has experienced rapid urban development and population growth since the 1960s, and Beijing's demand for water resources has increased daily. Over the years, the utilization of groundwater accounts for two-thirds of the total water supply in Beijing [32]. It is one of the few metropolises in the world that uses groundwater as the main source of its water supply [33]. With the long-term overexploitation of underground water, land subsidence has been developing rapidly in the Beijing area, and there is a trend in which the land subsidence funnel is connected into one piece [34]. By the end of 2015, the maximum cumulative settlement of Beijing plain area was approximately 1.4 metres, and the area with the cumulative settlement exceeding 1 metres reached 4000 km^2. Land subsidence has become a major threat to Beijing's urban construction planning and residential safety. Therefore, it is necessary to study the evolution rule and mechanism of land subsidence in the Beijing Plain.

At present, the problem of land subsidence is mainly concerned with its spatial distribution and formation factors, and the temporal problem of the mutation of land subsidence is rarely studied on the basis of long time series data. This study used ENVISAT ASAR and RADARSAT 2 to obtain the surface deformation information of the Beijing Plain area from 2004 to 2015; furthermore, to verify the accuracy, the research area was divided into 5,575 grids of 960 m by 960 m using the Fishnet tool of the ArcGIS platform. Then, the land subsidence information was obtained as a long time series for each grid using a space analysis tool. Subsequently, the Mann-Kendall test was carried out for each grid using Python, and the land subsidence mutation information of the Beijing Plain area was obtained based on the grid. Finally, combined with hydrogeology and basic geological conditions, we tried to analyse the causes of sudden changes in land subsidence.

2. Study area

Beijing, as the capital of China, is the centre of national politics, economy and culture and is an international metropolis with a population of nearly 20 million people. This area is located on the north-western edge of the North China Plain and occupies the region between 39.4°N, 115.7°E and 41.6°N, 117.4°E. In general, the topography is higher in the northwest and lower in the southeast. The geomorphologic features are divided into three parts: the western mountainous area, the northern mountainous area and the south-eastern plain (Figure 1). The total area of Beijing is 1,680,780 km^2, and the plain area covers 38% of the total area. From 2000 to 2011, Beijing suffered a continuous drought, with an average rainfall of only 459.11 mm.

Preprints (www.preprints.org) | NOT PEER-REVIEWED | Posted: 11 December 2018 doi:10.20944/preprints201812.0136.v1

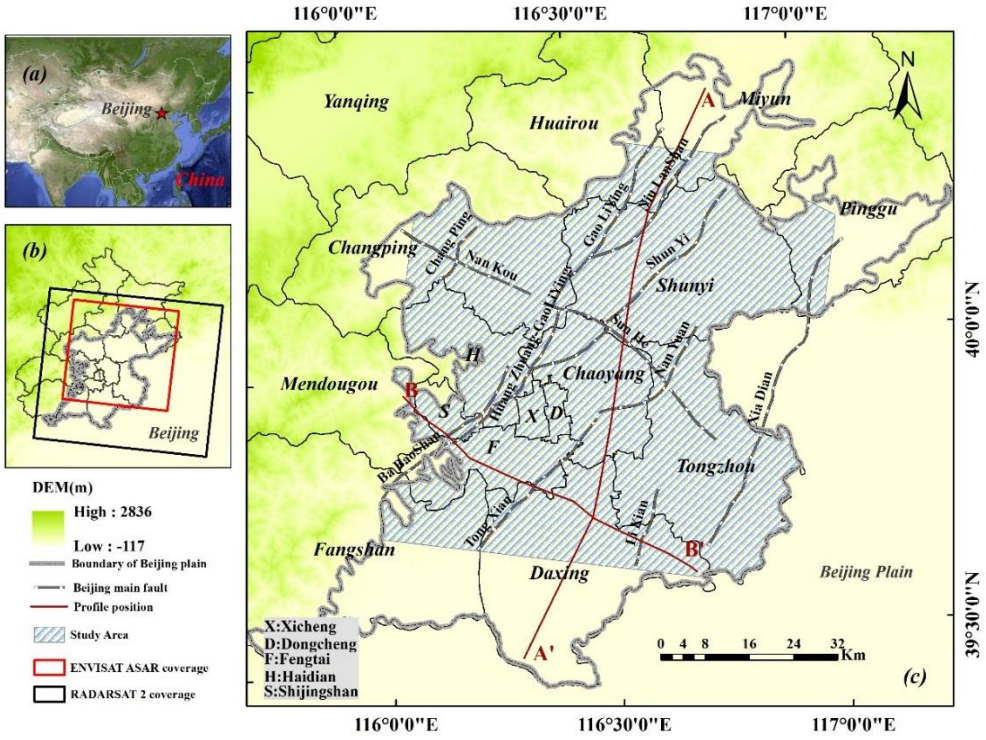

Figure 1. Geographic location of the study area. Figure a shows the location of Beijing. Figure b shows the range of the Beijing Plain. The red line represents the range of ENVISAT ASAR, and the black line represents the range of RADARSAT 2. Figure c shows the range of the study area. The grey dotted line represents the approximate fracture distribution of Beijing, and the dark red line represents the location of the hydrogeological profile.

The Beijing Plain area is formed by the combination of five major water systems (e.g., the Juma River system, Yongding River system, Wenyu River system, Chaobai River system and Jiyunhe River system)[35]. As shown in Figure 2, the Quaternary loose sediments in the study area are widely distributed. At the top of the alluvial fan, the Quaternary thickness is approximately 20 ~ 40 m, which is represented by a single gravel layer or a thin viscous soil layer covered with gravel [36]. In the lower part of the alluvial fan, the Quaternary loose sediment thickness gradually increases, and the gradation increases, and the particles gradually become thinner. The lithology gradually transitions to a point where sand, gravel, and viscous soil intersect each other and is dominated by viscous soil [37].There are many fractures in the study area, and the trend is mostly southeast-northwest and northeast-southwest.

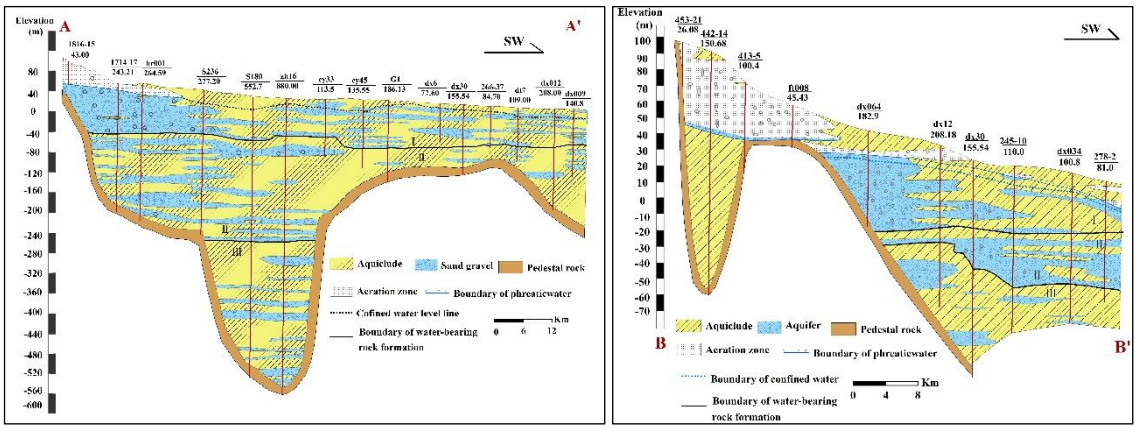

Figure 2. Hydrogeological profile.

 doi:10.20944/preprints201812.0136.v1

Land subsidence, as a surface response to the development, utilization and evolution of underground space, has become a global and multidisciplinary complex geological environment problem. Land subsidence first occurred in Beijing in 1935, and the main subsidence area was located in the area from Xidan to Dongdan. Since the 1970s, land subsidence in the Beijing Plain has entered a period of rapid development. In general, the subsidence area is divided into two major areas, i.e., north and south, and it has many subsidence centres [38]. "The North" is mainly distributed in the east and north of Beijing, including Chaoyang, Tongzhou, Changping, Haidian and Shunyi District. Among them, the Chaoyang and Tongzhou subsidence areas in the east of the plain are contiguous, and this area represents Beijing's most developed subsidence area [39]. The settlement rate of the four subsidence centres in the urban areas of Chaoyang (e.g., Jinzhan, Heizhuanghu and Sanjianfang) and Tongzhou exceeded 100 mm/year for many years. The subsidence centre in the north of the plain is found at the Changping Baxianzhuang and Haidian Xi Xiaoying areas. "The South" is mainly located in Daxing, and the settlement centre is in Lixian. Overall, the land subsidence is most developed in the eastern plain, followed by the northern region, and the south is mainly located in the vicinity of Hebei. As of the end of 2015, the area of land subsidence in Beijing reached 4842 km^2, with an average annual subsidence of 21.6 mm/year and an annual maximum value of nearly 141 mm/year.

3. Methodology

3.1. Data source

In this study, ENVISAT ASAR data and RADARSAT-2 data were selected to obtain the surface deformation information of Beijing from June 2003 to December 2015. ENVISAT is a solar synchronous polar orbiting satellite launched by the European Space Agency on March 1, 2002, and it has been out of contact since April 8, 2012; additionally, the largest sensor on it is a synthetic aperture radar. The ENVISAT ASAR sensor has an orbital altitude of 799.8 km, the operate band is a c-band with a wavelength of 5.6 cm, and the orbital repeat observation period is 35 days. This study obtained 47 images of the ascending orbit of ASAR data from June 2003 to August 2010, and the images covered most of the Beijing Plain except for the southernmost tip of Beijing. RADARSAT-2 is a radar satellite launched on December 14, 2007 by the Canadian Space Agency in collaboration with the MDA. It operates at the c-band with a wavelength of 5.6 cm, and the interval of orbital repeat observation period is 24 days. In this study, we obtained 48 RADARSAT-2 images that were from the descending orbit data from November 2010 to October 2015.

This study is based on Doris (Delft object-oriented radar interferometric software), StaMPS (Stanford method for persistent scatterers, StaMPS) and SARPROZ commercial software. After a series of tests, it was deduced that the time baseline threshold and space baseline threshold of the ASAR image from 2003 to 2010 were 500 days and 500 metres, respectively, and the interference processing generated 46 interference images. In addition, the time baselines and spatial baselines of the Radarsat-2 images during 2010-2015 were 500 days and 500 metres, respectively. During processing, a total of 266 interferometric image pairs were generated. In the process, the required external reference digital elevation model (DEM) data were the STRM3 (spatial resolution is 90 m) obtained by the National Aeronautics and Space Administration (NASA).

3.2. Processing of SBAS-InSAR based on StaMPS

In this study, StaMPS were selected to perform SBAS-InSAR processing on 47 scenes of ENVISAT ASAR data with a resolution of 30 m and a time span of 18 June 2003 to 25 October 2010. Small baseline interferometry (SBAS-InSAR) is a reliable method for studying long-term slow surface deformation, and this method was originally proposed by Berardino and Lanari in 2002[15]. The principle of this method is that the SAR image in the same study area is formed into several baseline pairs according to the sizes of the spatial baseline and time baseline. Thus, the small baseline data are combined into several sets. The purport is that within the set, the baseline of the interference pair is small; between sets, the baseline of the interference pair is larger. After obtaining the available small baseline interferogram, the surface deformation sequences of each set were obtained by the least

Preprints (www.preprints.org) | NOT PEER-REVIEWED | Posted: 11 December 2018 doi:10.20944/preprints201812.0136.v1

squares method. Finally, using the singular value decomposition method, multiple small baseline sets are jointly solved to obtain the deformation rate. In 2004, Lanari et al. proposed a method to further identify single-view SDFP pixels after recognizing multi-view SDFP pixels [16]. This method solves the loss-related issues that occur during the process of the standard small baseline method. The method adopted in this paper was proposed by Hooper in 2008, and the difference in the method involves identifying single-view SDFP (slowly decorrelated filtered phase) pixels in a single-view image [12].

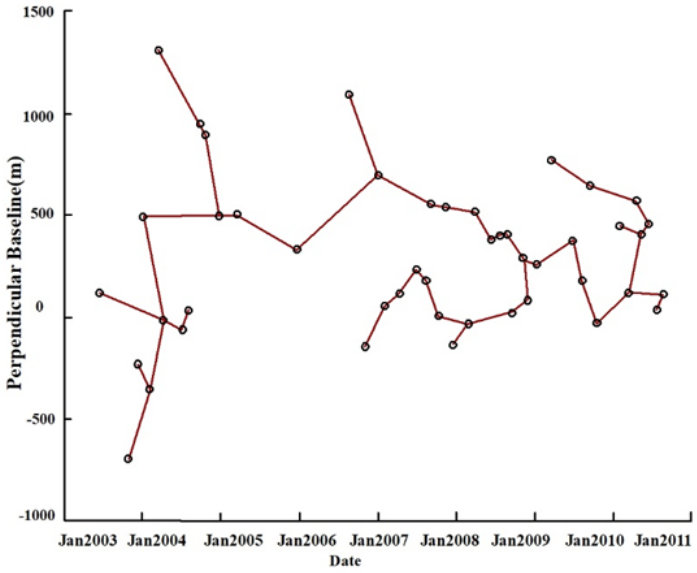

Figure 3. The small baseline segment from 2003 to 2010 was obtained by SBAS-InSAR technology.

3.3. Quisin-PSInSAR processing based on SARPROZ

In this study, the technical method of Quisin-PSInSAR in the SARPROZ software was selected to process 48-view RADARSAT-2 data. The RADARSAT-2 data resolution is 30 m, and the time span is from November 22, 2010 to November 20, 2015. The main steps include data set reading, main selection and registration, atmospheric phase analysis based on star topology and PS point deformation analysis based on custom structure.

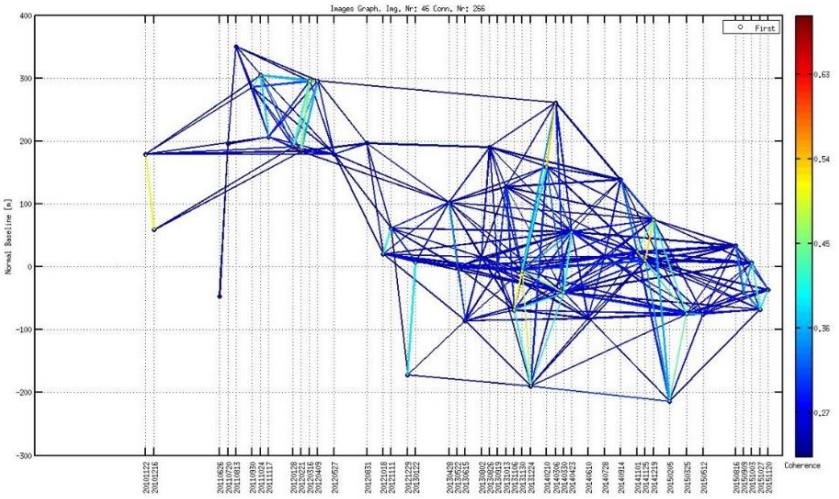

Figure 4. A small baseline set from 2010 to 2015 obtained by Quisin-PSInSAR technology.

3.4. Mann-Kendall mutation test

Preprints (www.preprints.org) | NOT PEER-REVIEWED | Posted: 11 December 2018 doi:10.20944/preprints201812.0136.v1

Mann-Kendall is a nonparametric statistical test method, also known as the non-distribution test. Its advantage is that it does not require samples to obey a certain distribution, and the results are not affected by a few outliers [40]. The Mann-Kendall method has been used by many scholars to analyse the trend changes of elements, such as precipitation, runoff and temperature, with time series [41-43]. In this paper, the test method is used to detect the change trend of land subsidence in the Beijing Plain. The method is summarized as follows:

For the time series X with n samples, construct an order list:

$$S_k = \sum_{i=0}^{k} r_i \qquad r_i = \begin{cases} 1, & x_i > x_j \\ 0, & else \end{cases} \qquad \text{j} = 1,2,\ldots,\text{i}$$

It can be seen that the order column Sk is the cumulative number of the number of values at time i greater than those at time j. Under the assumption of stochastic independence of time series, we define the following statistics:

$$UF_K = \frac{S_k - E(S_k)}{\sqrt{Var(S_k)}} \qquad \text{k=1,2,…,n}$$

Among them, UF1=0, E(Sk) and Var(Sk) are the mean and variance of cumulative Sk, respectively. When X1, X2,..., Xn are independent of each other and have the same continuous distribution, the following formula can be obtained:

$$\text{E}(S_k) = \frac{k(k-1)}{4} \qquad \text{Var}(s_k) = \frac{k(k-1)(2k+5)}{72}$$

where UFk is a standard normal distribution. It is a statistical sequence calculated in the order of time series X (x1, x2,..., xn). The significance level is given as α, and then the normal distribution table can be queried. If $|UF_k| > U\alpha$, it shows that the sequence has an obvious trend change. Similarly, the inverse order of UFk is calculated as UBk. The significance level selected in this study was α of 0.05, and the critical value was $U_{0.025} = \pm 1.96$.

4. Results

4.1. Acquisition of time series ground deformation information

Based on the surface deformation information monitored by SBAS-InSAR and Quisin-PSInSAR and using the ArcGIS space analysis platform, the ground settlement rate distribution map was obtained for the Beijing Plain. As shown in Figure 5, the spatial distribution of land subsidence in the Beijing Plain is wide, and the spatial difference is dramatic. The areas with serious subsidence are mainly in the east of Chaoyang, the northwest of Tongzhou, the south of Changping, the northwest of Shunyi and the south of Daxing. A plurality of settling funnels were formed in the study area, and they were connected to one another. PS points were obtained based on ENVISAT ASAR data. The maximum annual average sedimentation rate was 134 mm/year in the plain area, and the minimum annual average sedimentation rate was 1 mm/year. Among them, the area where the sedimentation rate was greater than 25 mm/year reached 1078.5 km², which accounted for 17.2% of the total area of the Beijing Plain. From 2011 to 2015, the number of PS points obtained based on RADARSAT-2 data was 100,515, the maximum average annual settlement rate in the plain area was approximately 141 mm/year, and the minimum settlement rate was approximately 2 mm/year. The area with a settlement rate greater than 25 mm/year reached 1,139 km², accounting for 17.8% of the area of the Beijing Plain. By the end of 2015, the area where the accumulative settlement of the Beijing Plain exceeded 300 mm reached 1,271 square kilometres, accounting for approximately 20% of the total area of the Beijing Plain.

Preprints (www.preprints.org) | NOT PEER-REVIEWED | Posted: 11 December 2018 doi:10.20944/preprints201812.0136.v1

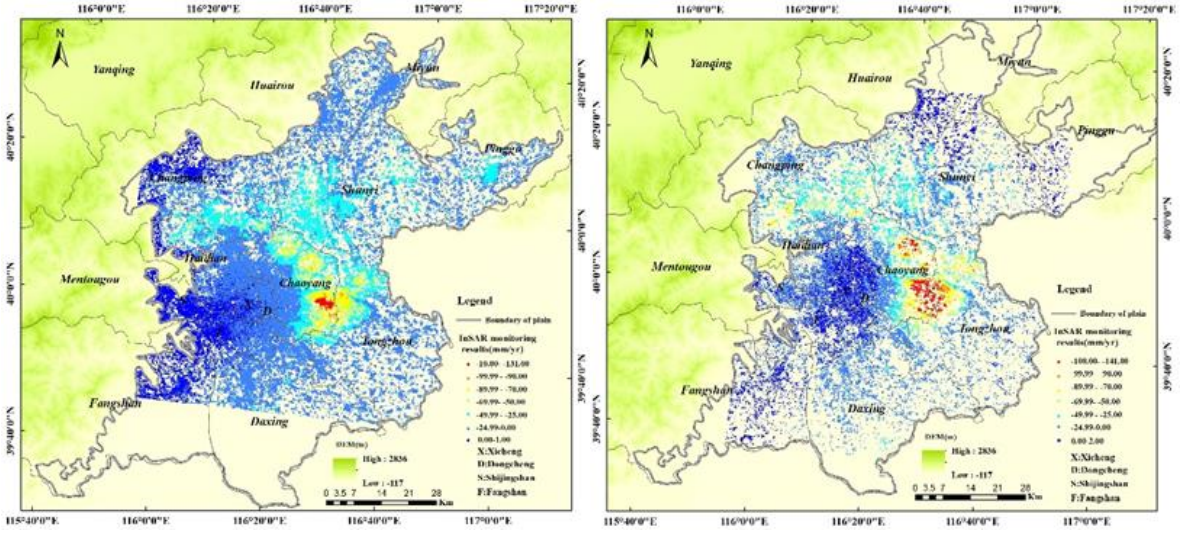

Figure 5. The average land subsidence rate map in the Beijing Plain. The left figure shows the average rate from 2004 to 2010, and the right figure shows the average rate from 2010 to 2015

4.2. InSAR accuracy verification

Because the shape variables obtained by SBAS-InSAR are the deformation values in the line of sight, to ensure the accuracy of verification, it is necessary to decompose them into vertical shape variables according to the incident angle of the sensor. This study was verified in two steps. First, the second-class level deformation isoline of 2007 was selected, and the results of SBAS-InSAR were preliminarily tested as a whole. Figure 6 shows that the settlement of the PS point obtained by SBAS-InSAR in 2007 has good consistency with the settlement of the level measurement in the overall spatial distribution.

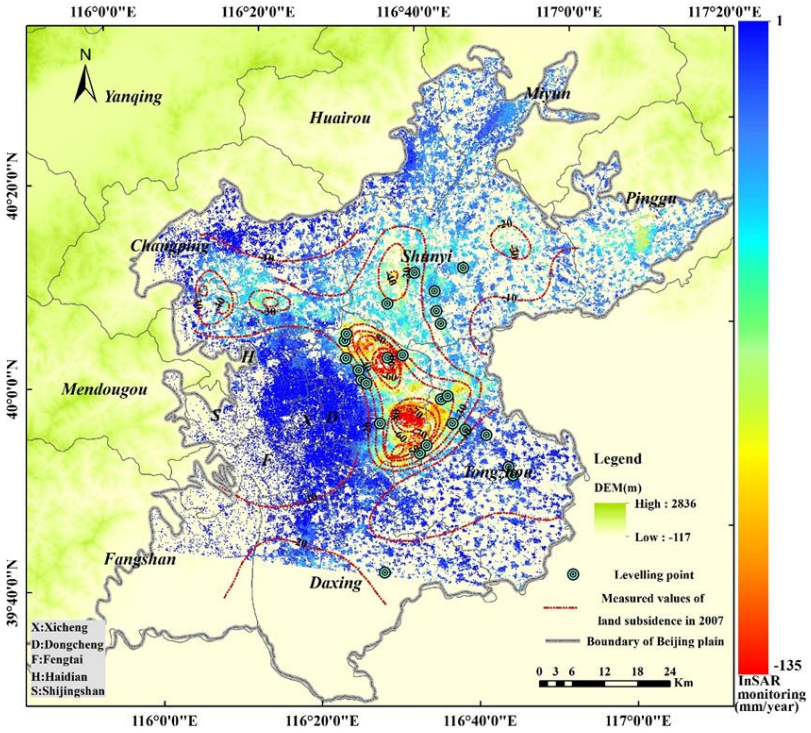

Figure 6. Verification map of land subsidence accuracy in the Beijing Plain area, in which the dark blue line represents the land subsidence contour of the levelling survey in 2007, and the green circle represents the position of the levelling point used for verification.

 doi:10.20944/preprints201812.0136.v1

Furthermore, the data of 24 levelling points from 2003 to 2013 were selected in this verification. The levelling points were taken as the original point, and all monitoring points within a radius of 150 m were extracted. The mean value of the extracted SDFP points and PS points were taken as the settlement estimation value and verified with the settlement of the levelling points. As shown in Figure 7, the correlation coefficient of the InSAR monitoring results and the level monitoring results from 2003 to 2010 was 0.95, the maximum absolute error was 17.9 mm/year, the minimum absolute error was 0.1 mm/year, and the standard deviation was 4 mm/year. From 2011 to 2013, the correlation coefficient of the InSAR monitoring results and the level monitoring results was 0.99, with a maximum absolute error of 17.3 mm/year, a minimum absolute error of 0.6 mm/year and a standard deviation of 3 mm/year. Although the PS point fail to coincide with the corresponding levelling points, they still reflect the high accuracy of the InSAR results.

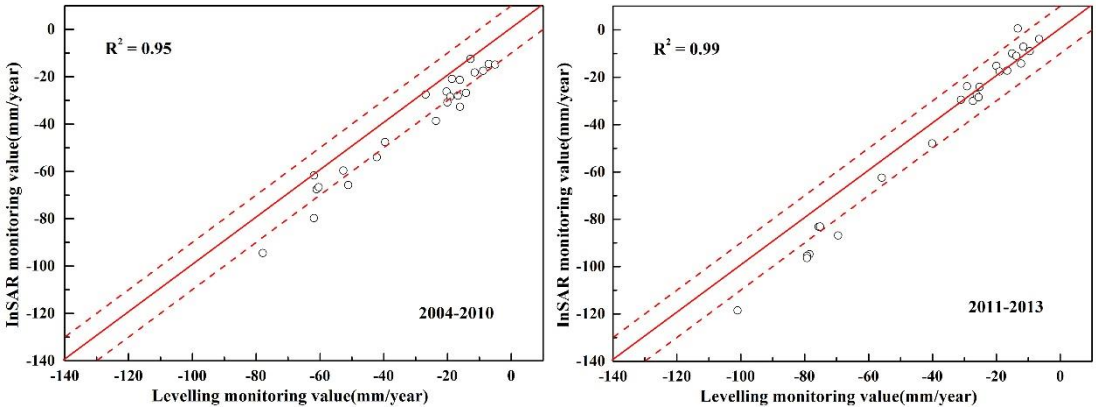

Figure 7. Comparison of InSAR-derived land subsidence rates and levelling measurement rate from 2003-2013. The figure on the left shows the accuracy verification from 2004 to 2010, and the figure on the right shows the accuracy verification from 2011 to 2013.

4.3. Mutation

First, after a series of tests, the research area was divided into 960×960 meter grids using the Fishnet tool of the ARCGIS platform (we divided the study area into 30 m×30 m, 60 m×60 m, 90 m×90 m...15,360 m×15,360 m grids, performed a mutation test on all of them and found the consistency of the trend. Finally, the grid of 960 m×960 m was chosen because it guaranteed that most of the grids (88%) had PS points of 2003-2015, and the grid can be refined as much as possible to express the research area.); in total, 5,575 grids were created. Second, according to the information of the PS points in 2004-2015 acquired by InSAR technology, the ground settlement information of each grid could be obtained based on the GIS platform. Finally, a Mann-Kendall mutation test was performed on each grid using Python, and the mutation information of ground settlement in the Beijing Plain area was obtained (as shown in Figure 8).

Preprints (www.preprints.org) | NOT PEER-REVIEWED | Posted: 11 December 2018 doi:10.20944/preprints201812.0136.v1

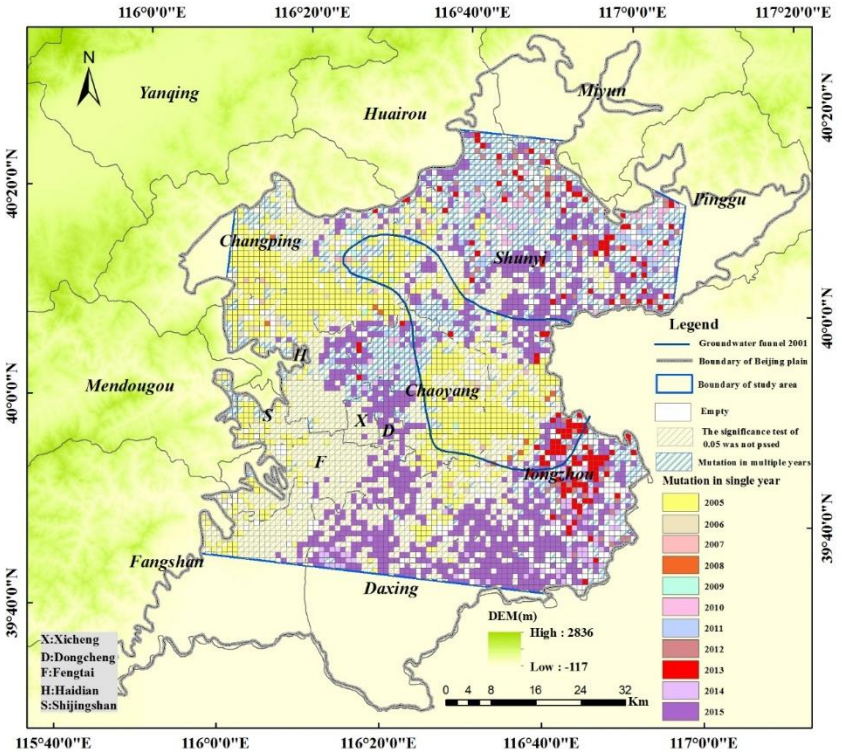

Figure 8. Land subsidence mutation information results of the Beijing Plain from 2004 to 2015. Among them, the dark blue line segment represents the 2001 underground water drop funnel, the grey line segment represents the boundary of the Beijing Plain, the white plane sign indicates that there is no continuous land subsidence from 2004 to 2015, the symbol of the grey slanted line indicates the grid that did not pass the significance test of 0.05, and the blue slanted grid represents the grid distribution with multiple mutations. Other monochromatic symbols represent grids with a single year of mutation.

In total, 4,887 grids had settlement information from 2004 to 2015, of which 3,792 grids passed the significance test (p=0.05). Among them, 2,744 grids had a mutation, and 1,048 grids had multiple mutations. Among the single-mutation grids, 1,344 grids mutated only in 2015, 915 grids mutated only in 2005, 152 grids mutated only in 2013 and fewer single-mutation grids occurred in other years.

Table 1-Beijing Plain Land subsidence Mutation Information

Order	Mutation years	Count	Order	Mutation years	Count
1	2015	1344	**18**	2011-2013	20
2	2005	915	**19**	2005,2007,2008	18
3	2013,2015	238	**20**	2010,2012,2013,2015	18
4	2013-2015	153	**21**	2007	16
5	2013	152	**22**	2011,2013,2015	16
6	2014	80	**23**	2005-2008	15
7	2012	72	**24**	2010,2012,2015	15
8	2011,2015	63	**25**	2008,2009	14
9	2012,2015	58	**26**	2005,2006,2009	13
10	2010	55	**27**	2006-2008	12
11	2011-2013,2015	51	**28**	2008	12
12	2011	47	**29**	2009	12
13	2012,2014,2015	40	**30**	2010,2012,2013	12
14	2006	39	**31**	2013,2014	12
14	2006	39	**31**	2013,2014	12

Order	Mutation years	Count	Order	Mutation years	Count
15	2010,2015	37	**32**	2010,2011,2015	10
16	2005,2008,2009	31	**33**	empty	1783
17	2005-2007	20	**34**	others	＜10
					In total 5575

Among the 1,048 grids with multiple mutation years of the land subsidence rate, the grid containing the mutations in 2015 contained the most, as it contained 768 grid cells with mutation. Among them, there were a large number of grids that were simultaneously mutated in 2013 and 2015, totalling 238. In addition, there were 153 grid mutations from 2013 to 2015 and 63 grid mutations in both 2011 and 2015. For the grid containing the 2005 mutations, 127 grid cells were mutated. In addition, the number of grids with multiple mutations in other years was relatively small.

5. Discussion

From the overall trend of the land subsidence rate mutation distribution map, the grid with the single-year mutation was mostly distributed in the middle and lower part of the ChaoBai River alluvial-diluvial fan and YongDing River alluvial-diluvial fan, and the grid with multiple-year mutations was mostly distributed at the top of the alluvial-diluvial fan. The reason may be that the groundwater level of the Quaternary system has dropped drastically, resulting in a decrease in pore water pressure in the overburden layer and a loss of water in the soil layer. However, in the middle and upper parts of the alluvial fan, most of the Quaternary diving or shallow confined water has good permeability, and the groundwater level fluctuates greatly due to the influence of precipitation. The rainfall quantity and the rainfall intensity are different in different seasons. These differences may cause the groundwater level in the middle and upper parts of the alluvial fan to experience relatively large fluctuations; thus, the grid with sudden land subsidence may be more variable. On the other hand, the Huairou emergency water source, the Machikou emergency water source, the Xishan emergency water source and the Pinggu emergency water source are all in the middle and upper parts of the alluvial fan. Affected by the distribution of exploitation, the groundwater level was greatly changed, resulting in greater fluctuations of land subsidence. Figure 8 illustrates that at the edge of the Quaternary groundwater drop funnel, the grids with mutations in the land subsidence rate are very variable. In the following sections, by considering the hydrogeological conditions, we will attempt to discuss the causes of grid changes in a single year and grid changes in multiple years.

5.1. Analysis of single-year mutation grid

In the 2744 land subsidence grids with a single mutation, 1344 grids occurred in 2015 (Figure 9). They are mainly distributed on the alluvial fans of the Chaobai River and Yongding River. First, the main reason may be that the “South-to-North Water Transfer Middle Line” project ran from the end of December 2014, and the water transfer year from 2014 to 2015 (the water transfer year refers to the annual water supply from November 1 to October 31) supplied 703 million cubic metres of water that was diverted to Beijing. Among them, 8 water plants used more than 2.2 million cubic metres of the "southern water" every day (accounting for 70% of the total water supply in Beijing's urban areas). At the same time, the Beijing municipal government has carried out a large-scale replacement project for self-provided wells, and the overall amount of groundwater extraction has decreased by 250 million cubic metres. This not only reduces the amount of groundwater exploitation

Preprints (www.preprints.org) | NOT PEER-REVIEWED | Posted: 11 December 2018 doi:10.20944/preprints201812.0136.v1

but also changes the distribution of groundwater exploitation, which may be one of the main reasons for the sudden change of the grid in 2015. Second, according to the Water Resources Bulletin, the average precipitation in Beijing in 2015 was 583 millimetres, which was 33% more than the 439 millimetres of precipitation recorded in 2014. In terms of the precipitation temporal distribution, the accumulated precipitation during the flood season (i.e., from June to September) was 447 millimetres, accounting for 77% of the annual precipitation, and this value was 8% less than the annual average of 488 millimetres. This result means that the excessive rainfall is lower, and the effective supply of precipitation is greater. Third, according to the data of the Beijing Geological Environment Monitoring Station, 150 million cubic metres of water were recharged to the Beijing Plain every year from 2015 to 2020. Although the depth of recharge is typically approximately 50 metres, groundwater systems are interlinked, which may also be one of the reasons for the sudden change of the grid in 2015. Finally, according to the Beijing subway official website, three subways were opened in 2015, and the dynamic load is one of the causes of land subsidence in Beijing. In addition, six subways were newly built in Beijing during the year, and the groundwater level will be artificially lowered during the subway construction period. This event may have caused some grids to mutate in that year.

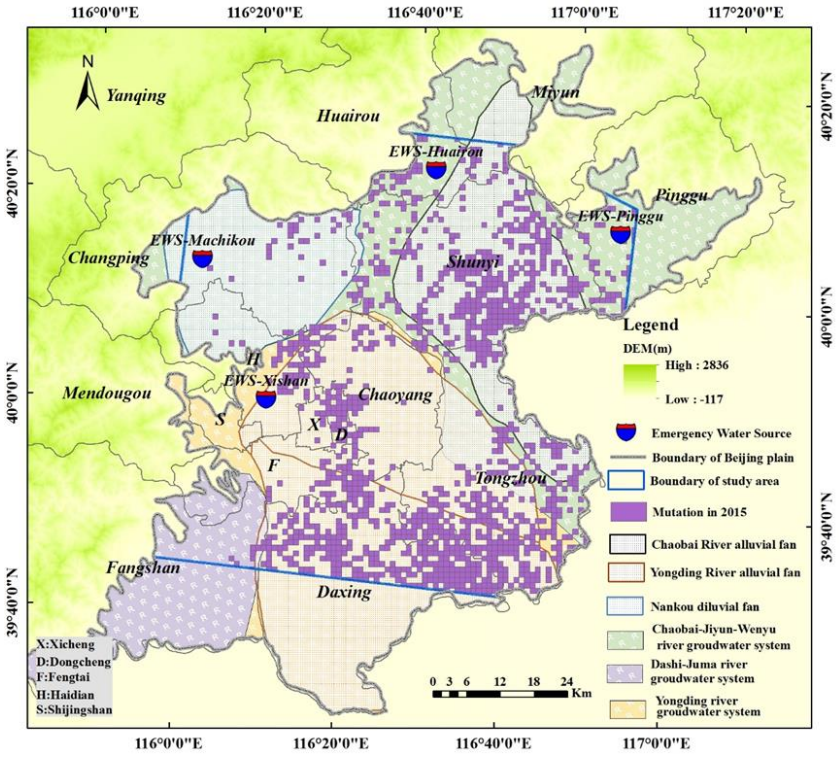

Figure 9. Spatial distribution of a single mutation grid in 2015. Among them, the blue-red dot pattern represents the emergency water source in the study area, the purple grid is the location where the land subsidence rate is abrupt only in 2015, and the surface pattern containing the brown dots represents the Yongding River alluvial fan range. The surface pattern of the black points represents the range of the Chaobai River alluvial fan.

Figure 10 shows that a single abrupt change in land subsidence occurred in 2005, mostly in the upper and middle parts of the Yongding River alluvial fan, the Nankou alluvial fan and the lower part of the Chaobai River alluvial fan. From the perspective of the district, most of these sits were located in southeast Haidian, southeast Changping, southeast Chaoyang and northeast Tongzhou.

Preprints (www.preprints.org) | NOT PEER-REVIEWED | Posted: 11 December 2018 doi:10.20944/preprints201812.0136.v1

For the alluvial-diluvial fan of the Yongding River corresponding to the grid location, the reasons for the sudden change in 2005 may be as follows. First, the Xishan emergency water source area was built in 2005 in the area of groundwater exploitation. The mining target layer of the emergency water source area contains Quaternary groundwater, which is located in the upper part of the alluvial fan of the Yongding River. It is mainly composed of a single layer of sand and gravel with good permeability. The sudden increase in groundwater exploitation will lead to the sudden drop of the groundwater level, which may cause the sudden change of the corresponding grid land subsidence. According to the Water Resources Bulletin, the precipitation of the Yongding River was the lowest, at only 386 mm. This result shows that the groundwater system of the Yongding River has little recharge, which may be one of the reasons for the sudden change of land subsidence of the alluvial fan of the Yongding River in 2005.

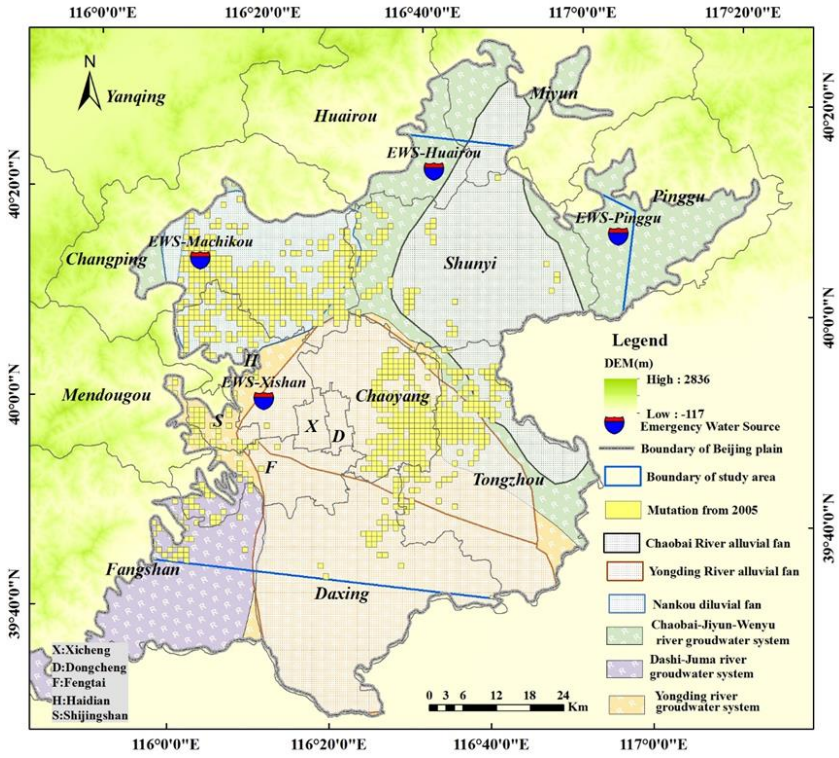

Figure 10. Spatial distribution of a single mutation grid in 2005. Among them, the yellow grid represents the locations where the land subsidence rate changed in only 2005.

The reason for the sudden change of land subsidence of Nankou alluvial fan in 2005 is that, on the one hand, the Wenyu River groundwater system (where the Nankou alluvial fan is located) and the Chaobai River groundwater system belong to a subsystem of the same groundwater system, which has a certain boundary and hydraulic connection. However, the Huairou emergency water source located at the top of the Chaobai River groundwater system started operating in August 2003. After a period of operation, the water source will destroy the balance of the groundwater system, and the nearby Wenyu River groundwater system will supply it, which may have led to the sudden change at the southern mouth diluvial fan area at the lower part in 2005. Second, in terms of groundwater recharge, from the perspective of precipitation, the depositional particles at the location of the Nankou diluvial fan were larger and had better permeability, and the groundwater level fluctuated greatly under the influence of precipitation. The average annual precipitation in Beijing

Preprints (www.preprints.org) | NOT PEER-REVIEWED | Posted: 11 December 2018 doi:10.20944/preprints201812.0136.v1

was 468 millimetres in 2005, which was 13% less than that of the same period in 2004. From the regional distribution of precipitation, the precipitation in mountainous areas was greater than that in plain areas, and the former mountainous areas in the northwest and southwest had more precipitation. Part of the rainstorm centre was located in Nankou District. This result shows that in 2005, the region not only supplied less but also supplied less effectively. For a small portion of the grid that is found in the lower part of the alluvial-diluvial fan of the Chaobai River, there may have been very little precipitation in that year. On the other hand, it is possible that there was a Huairou emergency water source in the upper part of the area (the water source was officially operated at the end of 2003) and a Pinggu water source (the water source started operation in August 2004), and the exploitation of the emergency water sources will cause a rapid decline in the nearby groundwater level. Thus, the direction of recharge-runoff-discharge of the groundwater system changes, which indirectly affects the groundwater level in the lower part of the alluvial fan. In summary, the reason for the sudden change in land subsidence in 2005 may have been the increase in groundwater exploitation and the small amount of effective precipitation replenishment.

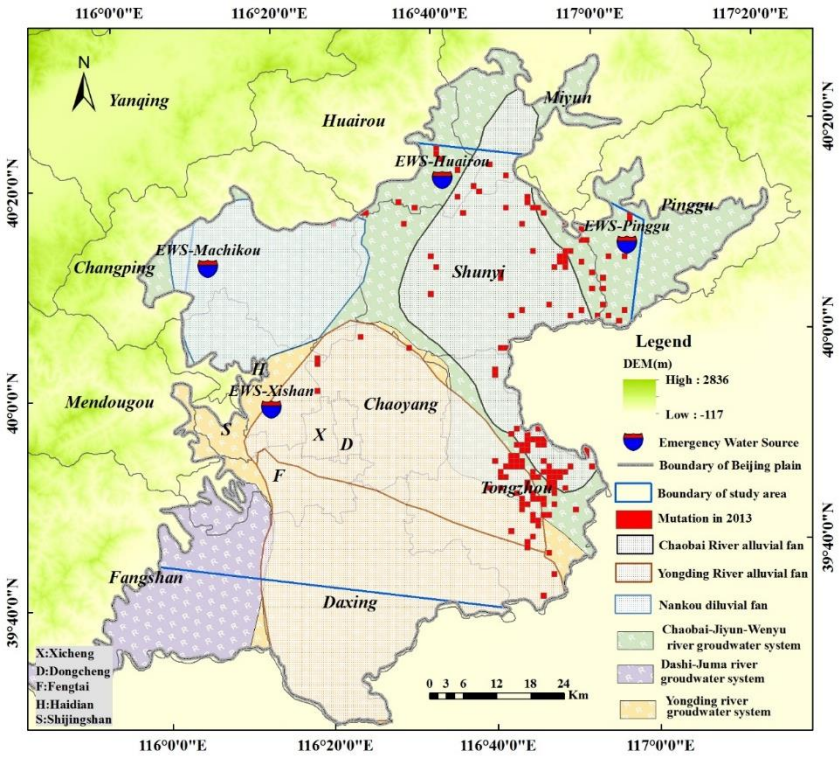

Figure 11. Spatial distribution of a single mutation grid in 2013. Among them, the red grid represents the locations where the land subsidence rate changed only in 2013.

The 152 grids where land subsidence changed abruptly in 2013 were mainly distributed in the Chaobai River alluvial fan (as shown in Figure 11). From the administrative area, they are mainly distributed in Tongzhou District. The reason is that in September 2012, the Beijing municipal government announced the selection of Tongzhou District as a new city deputy centre. After 2013, Tongzhou developed rapidly. Second, the Tongzhou area became dramatically "higher" and "larger". However, the increasing number of buildings and the growing height were one cause of Beijing's land subsidence. Third, after 2013, the density of both roads and subways in the Tongzhou area

Preprints (www.preprints.org) | NOT PEER-REVIEWED | Posted: 11 December 2018 doi:10.20944/preprints201812.0136.v1

increased dramatically. In summary, the above three reasons may have caused the sudden change in land subsidence in some areas of Tongzhou in 2013.

5.2. Analysis of grids with multiple land subsidence mutation years

The 1,048 grids with multiple mutation years were mainly distributed at the top of the alluvial fan, the boundary of the groundwater system, and the edge of the groundwater funnel. The largest number of grids containing mutations in 2015 was 768, followed by 152 grids that contained mutations in 2005. The grid that contained multiple changes in years that include 2015 was mainly distributed at the top of the Chaobai River alluvial fan, near the Pinggu emergency water source, at the top of the Yongding River alluvial fan and at the bottom of the Chaobai River alluvial fan (as shown in Figure 12).

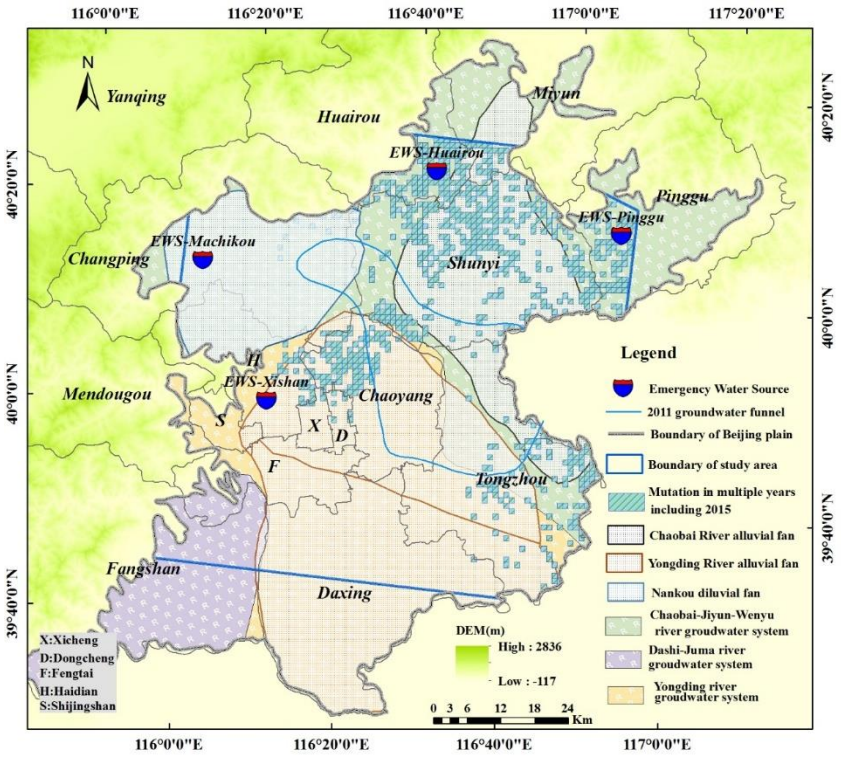

Figure 12. The spatial distribution of multiple mutation grids that include 2015. Among them, the blue fringe grid represents the location where the land subsidence rate has mutated more than 1 year and contained the year 2015.

In terms of the administrative area, the sites were mainly distributed in southern Huairou, northern Shunyi, southwest of Pinggu and eastern Tongzhou. The reasons are analysed as follows: first, after the water diversion project of the South-to-North water transfer project at the end of 2014, the underground water was reduced in many places, such as the Huairou emergency source, Chaobai River greening water source well and Pinggu emergency water source. The "southern water" was used to recharge groundwater in well-penetrated areas (such as in the Huairou emergency water source and Pinggu emergency water source area), and relevant departments have completed the replacement of several self-providing wells, which not only reduces the amount of groundwater exploitation and optimizes the groundwater exploitation layout but also effectively recharges and conserves the groundwater system. Second, the precipitation in this region was higher in 2015 than

Preprints (www.preprints.org) | NOT PEER-REVIEWED | Posted: 11 December 2018 doi:10.20944/preprints201812.0136.v1

in the past 10 years, and the groundwater recharge was relatively sufficient. Third, the Beijing government has taken a series of measures to save water and strengthen the use of reclaimed water, which indirectly protects groundwater resources.

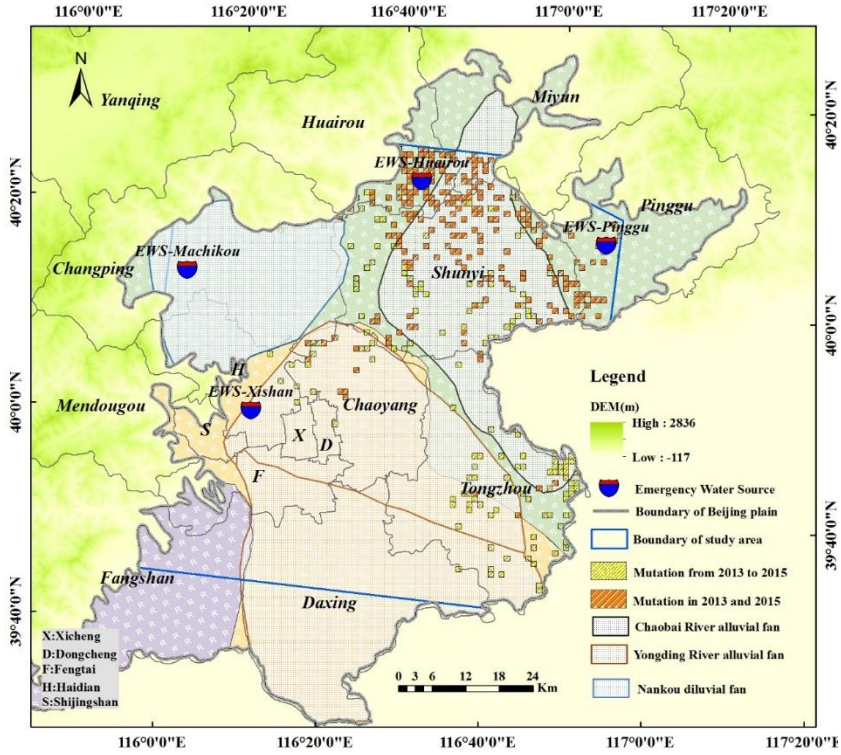

Figure 13. The spatial distribution of multiple mutation grids that contained 2013 and 2015. Among them, the yellow fringe grid represents the location where the land subsidence rate has mutated from 2013 to 2015, and the yellow orange grid represents the location where the land subsidence rate mutated in both 2013 and 2015.

Among the grids with multiple mutations including a mutation in 2015, the number of grids with simultaneous mutations was highest in 2013 and 2015, at 238 (as shown in Figure 13). The spatial distribution was almost completely in the upper and middle parts of the alluvial-diluvial fan of the Chaobai River. From the perspective of administrative regions, most of these sites were distributed in the southwest of Huairou, the south of Miyun, the west of Pinggu, Tongzhou District and the area of Shunyi. The reason for the sudden change in 2013 may be the long-term overexploitation of emergency water sources, which led to the imbalance of the groundwater system.

Subsequently, there were 153 grids with multiple mutation years in 2013-2015, and they were mainly distributed in the Tongzhou area. The reason may be that after September 2012, Tongzhou was selected as the city deputy centre of Beijing. From 2013 to 2015, the Tongzhou area has been expanding continuously, the demand for water resources has been increasing, and its dynamic and static load density has been increasing. This is the reason for the great change in land subsidence in Tongzhou during this period. The number of grids with multiple-year mutations in other years is very small, and no more analysis must be performed here.

6. Conclusion

 doi:10.20944/preprints201812.0136.v1

This study used 47 ENVISAT ASAR data from June 2003 to October 2010 and 48 RADARSAT-2 data from November 2010 to December 2015. The Doris/StaMPS algorithm and commercial SARPROZ software were used to analyse the SAR data. The surface deformation information of the Beijing Plain was obtained from 2004 to 2015, and its accuracy was verified. On the ARCGIS platform, the Fishnet tool was used to divide the research area into a grid of 960 by 960 metres, and the ground settlement information of each grid was obtained from 2004 to 2015 using spatial analysis technology. Using Python, the Mann-Kendall test was carried out for each grid, and the change characteristics of ground settlement were obtained for the Beijing Plain area. The reasons for the mutations were analysed, and the following conclusions were obtained.

1) From 2004 to 2015, the spatial distribution of land subsidence in the Beijing Plain area was quite different, and many subsidence funnels were formed in the area. From 2004 to 2010, the average ground settlement rate in the study area was 134 mm/year, and from 2010 to 2015, the average ground settlement rate was 141 mm/year. By the end of 2015, the accumulative settlement of the Beijing Plain area exceeding 300 mm, and the area reached 1,271 square kilometres, accounting for approximately 20% of the total area of the Beijing Plain.

2) There are two kinds of land subsidence mutation grids, including single-year mutations and multiple-year mutations. Among them, the number of single-year grid changes was 2,744, and they were mainly distributed in the middle and lower parts of the alluvial-diluvial fans of the Yongding River and Chaobai River. The number of multiple-year grid mutations was 1,048, and they were mainly distributed in the middle and upper parts of the alluvial fan, near the emergency water source and at the edge of the underground water funnel.

3) Among the 4,887 grids with ground settlement information from 2004 to 2015, 3,792 grids passed the significance test. Among them, the number of grids containing land subsidence mutations in 2015 was the highest, reaching as high as 2,112 grids and accounting for 56% of the number of grids; this value was followed by 995 grids containing mutations in 2005, which accounted for 27% of the number of grid passings.

4) The grids that changed in 2015 were mainly distributed in the middle and lower parts of the alluvial-diluvial fans of the Chaobai River and Yongding River. The main reason may be that after the "southern water" entered Beijing at the end of 2014, the amount of underground water was reduced, and the relevant departments carried out underground water recharges; as a result, they replaced a large number of self-providing wells and optimized the distribution of underground water exploitation. In addition, the effective precipitation amount in the Beijing Plain was relatively large in 2015. Most grid changes occurred in 2015, which also suggested that the "southern water" entering Beijing had a certain role in alleviating land subsidence in Beijing.

5) It cannot be ignored that in 2013, the number of sudden changes in the single-year land subsidence grids was 152, while in 2013-2015, the number of sudden changes was 153, and they were mainly distributed in Tongzhou. The main reason for this difference may be that after Tongzhou was selected as the sub-centre of Beijing in September 2012, the rapid development of Tongzhou in a short period was one of the main causes of the sudden change in land subsidence during 2013-2015. This further supports that the density of dynamic loads and static loads increased sharply, which was one of the reasons for the uneven land subsidence in the Beijing Plain.

 doi:10.20944/preprints201812.0136.v1

Finally, it should be added that to some extent, the "southern water" in Beijing mitigates the trend of rapid development of Beijing land subsidence, but the land subsidence phenomenon in Beijing is still not negligible. Next, we will use more multi-source SAR and GRACE data [44], optimize the algorithm, adopt different software platforms, improve the monitoring density and accuracy of land subsidence in Beijing, and analyse its evolution mode from different perspectives. We will thoroughly combine hydrogeology, and basic geological conditions and geophysical exploration technologies; additionally, we will combine different mathematical methods and adopt interdisciplinary methods to further analyse the cause formation mechanism of land subsidence in the Beijing Plain.

Author Contributions: Lin Guo performed the experiments, analyzed the data and wrote the paper. Huili Gong and Lin Zhu provided crucial guidance and support through the research. Feng Zhu and Chaofan Zhou contributed significantly to the validation work and data interpretation. Yike Sun made important suggestions on data processing.

Funding: This work was supported by the National Natural Science Foundation of China under Grant (number D0107/41130744 ,D0107/4177010971 and D0107/41171335) and the National Basic Research Program of China (973 Program) under Grant (number 2012CB723403)..

Acknowledgments: We thank both the European Space Agency (ESA) and Canadian Space Agency for their great efforts in developing and distributing the remotely-sensed SAR data. We also thank the China Geological Survey (CGS) for the leveling data released to the public. We also thank for National Aeronautics and Space Administration (NASA) for making SRTM DEM data available. Moreover, the provision of the Doris and StaMPS for data processing by TUDelft is also gratefully acknowledgsed.

Conflicts of Interest: The authors declare no conflict of interest.

References

1. Chaussard, E.; Wdowinski, S.; Cabral-Cano, E.; Amelung, F. Land subsidence in central Mexico detected by alos insar time-series. *Remote Sensing of Environment,* (**2014**). *140(1),* 94-106.
2. Gong, H.; Pan, Y.; Zheng, L.; Li, X.; Zhu, L.; & Zhang, C. Long-term groundwater storage changes and land subsidence development in the North China Plain (1971–2015). (**2018**). *Hydrogeology Journal.* DOI.*10.1007/s12665-015-4131-2*
3. Gao, M.; Gong, H.; Chen, B.; Li, X.; Zhou, C.; Shi, M. Regional land subsidence analysis in eastern Beijing Plain by insar time series and wavelet transforms. *Remote Sensing,* (**2018**). *10(3),* 365.
4. Ng, H. M.; Ge, L.; Li, X.; Abidin, H. Z.; Andreas, H.; Zhang, K. Mapping land subsidence in Jakarta, Indonesia using persistent scatterer interferometry (psi) technique with Alos Palsar. *International Journal of Applied Earth Observations & Geoinformation,* (**2012**). *18,* 232-242.
5. Strozzi, T.; Caduff, R.; Wegmüller, U.; Raetzo, H.; Hauser. Widespread surface subsidence measured with satellite sar interferometry in the Swiss alpine range associated with the construction of the gotthard base tunnel. *Remote Sensing of Environment,* M. (**2017**). *190,* 1-12.
6. Xue, Y. Q.; Zhang, Y.; Ye, S. J.; Wu, J. C.; Li, Q. F. Land subsidence in China. *Environmental Geology,* (**2005**). *48(6),* 713-720.
7. Zhang, Y.; XUE, YuQun; WU, JiChun; & YE, et al. Characteristics of aquifer system deformation in the southern Yangtse Delta, China. *Engineering Geology,* (**2007**). *90(3),* 160-173.
8. Ye, S.; Xue, Y.; Wu, J.; Yan, X.; Yu, J. Progression and mitigation of land subsidence in China. *Hydrogeology Journal,* (**2015**). *24(3),* 1-9.
9. Yin, J.; Yu, D.; Wilby, R. Modelling the impact of land subsidence on urban pluvial flooding: a case study of downtown Shanghai, China. *Science of the Total Environment,* (**2016**). *544,* 744-753.
10. Liu, P.; Li, Q.; Li, Z.; Hoey, T.; Liu, Y.; Wang, C. Land subsidence over oilfields in the Yellow River Delta. *Remote Sensing,* (**2015**). *7(2),* 1540-1564.
11. Zhu, L.; Gong, H.; Li, X.; Wang, R.; Chen, B.; Dai, Z. Land subsidence due to groundwater withdrawal in the northern Beijing Plain, China. *Engineering Geology,* (**2015**). *193,* 243-255.
12. Hooper, A. A multi-temporal insar method incorporating both persistent scatterer and small baseline approaches. *Geophysical Research Letters,* (**2008**). *35(16),* 96-106.
13. Elliott, J. R.; Biggs, J.; Parsons, B.; Wright, T. J. Insar slip rate determination on the altyn tagh fault, northern Tibet, in the presence of topographically correlated atmospheric delays. *Geophysical Research Letters*, (**2008**). *35(12),* 82-90.
14. Amelung, F.; Galloway, D. L.; Bell, J. W.; Zebker, H. A.; Laczniak, R. J. Sensing the ups and downs of Las Vegas: insar reveals structural control of land subsidence and aquifer-system deformation. *Geology,* (**1999**) *27(6),* 483-486.
15. Berardino, P.; Fornaro, G.; Lanari, R.; Sansosti, E. A new algorithm for surface deformation monitoring based on small baseline differential sar interferograms. *IEEE Transactions on Geoscience & Remote Sensing*, (**2002**). *40(11),* 2375-2383.
16. Lanari, R.; Mora, O.; Manunta, M.; Mallorquí, J. J.; Berardino, P.; Sansosti, E. A small-baseline approach for investigating deformations on full-resolution differential sar interferograms. *Geoscience & Remote Sensing IEEE Transactions on,* (**2004**). *42(7*), 1377-1386.
17. Hooper, A.; Zebker, H.; Segall, P.; Kampes, B. A new method for measuring deformation on volcanoes and other natural terrains using insar persistent scatterers. *Geophysical Research Letters,* (**2004**).*31(23),* L23611.
18. Sansosti, E. A small-baseline approach for investigating deformations on full-resolution differential sar interferograms. *Geoscience & Remote Sensing IEEE Transactions on,* (**2004**).*42(7),* 1377-1386.
19. Lanari, R.; Casu, F.; Manzo, M.; Zeni, G.; Berardino, P.; Manunta, M. An overview of the small baseline subset algorithm: a dinsar technique for surface deformation analysis. *Pure & Applied Geophysics,* (**2007**).*164(4),* 637-661.
20. Hooper, A. A multi-temporal insar method incorporating both persistent scatterer and small baseline approaches. *Geophysical Research Letters,* (**2008**).*35(16)*, 96-106.
21. Guzzetti, F.; Manunta, M.; Ardizzone, F.; Pepe, A.; Cardinali, M.; Zeni, G. Analysis of ground deformation detected using the sbas-dinsar technique in Umbria, central Italy. *Pure & Applied Geophysics,* (**2009**). *166(8-9),* 1425-1459.
22. Casu, F.; Manzo, M; Lanari, R. A quantitative assessment of the sbas algorithm performance for surface deformation retrieval from dinsar data. *Remote Sensing of Environment,* (**2006**). *102(3),* 195-210.

23. Lanari, R.; Berardino, P.; Bonano, M.; Casu, F.; Manconi, A.; Manunta, M.. Surface displacements associated with the L'Aquila 2009 mw 6.3 earthquake (central Italy): new evidence from sbas-dinsar time series analysis. *Geophysical Research Letters*, (**2010**). *37(20).*L044780
24. Dehghani, M.; Valadan Zoej, M. J.; Entezam, I.; Mansourian, A.; Saatchi, S. Insar monitoring of progressive land subsidence in neyshabour, northeast iran. *Geophysical Journal International,* (**2010**). 186(1), 47-56.
25. Zhao, C.; Lu, Z.; Zhang, Q.; Fuente, J. D. L. Large-area landslide detection and monitoring with alos/palsar imagery data over northern California and southern Oregon, USA. *Remote Sensing of Environment,* (**2012**).*124(9),* 348-359.
26. Chaussard, E.; Amelung, F.; Abidin, H.; Hong, S. H. Sinking cities in Indonesia: Alos Palsar detects rapid subsidence due to groundwater and gas extraction. *Remote Sensing of Environment,* (**2013**). *128(1),* 150-161.
27. Polcari, M.; Albano, M.; Saroli, M.; Tolomei, C.; Lancia, M.; Moro, M. Subsidence detected by multi-pass differential sar interferometry in the Cassino Plain (central Italy) Remote Sensing, (**2014**). *6(10),* 9676-9690.
28. Qinhui Zhang; Xiangyong Zhao; Renbing Sun; Haosu Luo. Land subsidence and ground fissures in Xi'an, China 2005–2012 revealed by multi-band insar time-series analysis. *Remote Sensing of Environment*, (**2014**).*155,* 366-376.
29. Grzovic, M.; Ghulam, A. Evaluation of land subsidence from underground coal mining using timesar (sbas and psi) in springfield, Illinois, USA. *Natural Hazards,* (**2015**). *79(3),* 1739-1751.
30. Torbjörn E. Törnqvist.; Wallace, D. J.; Storms, J. E. A.; Wallinga, J.; Dam, R. L. V.; Blaauw, M. Mississippi delta subsidence primarily caused by compaction of holocene strata. *Nature Geoscience,* (**2008**). *1(3),* 173-176.
31. Tomas, R.; Herrera, G.; Cooksley, G.; Mulas, J. Persistent scatterer interferometry subsidence data exploitation using spatial tools: the vega media of the Segura River Basin case study. *Journal of Hydrology*, (**2011**). *400(3),* 411-428.
32. Gong, H.; Pan, Y. Spatio-temporal variation of groundwater recharge in response to variability in precipitation, land use and soil in Yanqing Basin, Beijing, China. *Hydrogeology Journal*, (**2012**). *20(7),* 1331-1340.
33. Chen, B.; Gong, H.; Lei, K.; Zhu, L.; Gao, M. Characterization and causes of land subsidence in Beijing, China. *International Journal of Remote Sensing,* (**2017**). *38(3),* 808-826.
34. Zhou, C.; Gong, H.; Chen, B.; Zhu, F.; Duan, G., Gao, M. Land subsidence under different land use in the eastern Beijing Plain, China 2005-2013 revealed by insar timeseries analysis. (**2016**). *Mapping Sciences & Remote Sensing,* 53(6), 671-688.
35. Zhou, C.; Gong, H.; Chen, B.; Li, J.; Gao, M.; Zhu, F. Insar time-series analysis of land subsidence under different land use types in the eastern Beijing Plain, China. *Remote Sensing,* (**2017**). *9(4),* 380.
36. Zhai, Y.; Wang, J.; Teng, Y.; Zuo.R. Hydrogeochemical and isotopic evidence of groundwater evolution and;recharge in aquifers in Beijing Plain, China. *Environmental Earth Sciences,* (**2013**).*69(7),* 2167-2177.
37. Xie, Z.H.; Xu, M.J.; Xing, G.Z. Groundwater of Beijing; Zhang, A.J., Ed.; China Land Press: Beijing, China, 2008.(In Chinese)
38. Chen, B.; Gong, H.; Li, X.; Lei, K.; Zhang, Y.; Li, J. Spatial-temporal characteristics of land subsidence corresponding to dynamic groundwater funnel in Beijing municipality, China. *Chinese Geographical Science*, (**2011**) 21(6), 753-764.
39. Chen, M.; Tomás, R.; Li, Z.; Motagh, M.; Li, T.; Hu, L. Imaging land subsidence induced by groundwater extraction in Beijing (China) using satellite radar interferometry. *Remote Sensing,* **(2016)**. *8(6).* DOI.org/10.3390/rs8060468
40. Hamed, K. H.; Rao, A. R. A modified mann-kendall trend test for autocorrelated data. *Journal of Hydrology*, (**1998**). *204(1-4*), 182-196.
41. Kahya, Ercan; Kalayci, S.; Serdar. Trend analysis of streamflow in Turkey. *Journal of Hydrology*, (**2004**). *289(1)*, 128-144.
42. Danneberg, J. Changes in runoff time series in Thuringia, Germany - mann-kendall trend test and extreme value analysis. *Advances in Geosciences,* **(2012).** *31(31)*, 49-56.
43. Ding, Y.; Wang, Z.; Sun, Y. Inter-decadal variation of the summer precipitation in east china and its association with decreasing Asian summer monsoon. *International Journal of Climatology*, (**2010**). 28(9), 1139-1161.

44. Pan, Y.; Zhang, C.; Gong, H.; Pat J.-F. Yeh.; Shen, Y.; Guo, Y. Detection of human-induced evapotranspiration using grace satellite observations in the Haihe River Basin of China. *Geophysical Research Letters*, (**2017**). *44*. DOI.org/10.1002/2016GL071287